



UNIVERSIDADE ESTADUAL DE CAMPINAS SISTEMA DE BIBLIOTECAS DA UNICAMP REPOSITÓRIO DA PRODUÇÃO CIENTIFICA E INTELECTUAL DA UNICAMP

Versão do arquivo anexado / Version of attached file:

Versão do Editor / Published Version

Mais informações no site da editora / Further information on publisher's website:

https://link.springer.com/article/10.1007/s10494-023-00456-9

DOI: https://doi.org/10.1007/s10494-023-00456-9

Direitos autorais / Publisher's copyright statement:

©2023 by Springer. All rights reserved.

RESEARCH



Acoustic Radiation of a Simplified Jet-Flap-Thrust Gate Configuration: Numerical and Experimental Investigation

José R. L. N. Sirotto¹ · Julio A. Cordioli² · Petrônio A. S. Nogueira³ · André V. G. Cavalieri⁴ · Maicon Secchi⁵ · William R. Wolf⁶

Received: 27 February 2023 / Accepted: 4 July 2023 © The Author(s), under exclusive licence to Springer Nature B.V. 2023

Abstract

A comparative study of the acoustic far-field radiation of a subsonic jet near a folded plate with an opening, intended to represent a flapped wing with thrust gate, is presented in this work. Three openings with different widths were used to evaluate experimentally the influence of the gaps in the far-field noise radiation, for two folding angles. Boundary Element Method simulations with a wavepacket model which represents the jet acoustic source are used to calculate the far-field noise. Numerical simulation results are compared with experimental measurements and show similar trends in terms of acoustic radiation. Through parametric simulations, it was also possible to estimate that opening widths greater than one jet diameter do not contribute significantly to reducing the far-field noise. The results show that even the smallest tested openings were able to reduce the far-field noise for the tested positions.

List of Symbols

- D Nozzle exit diameter
- G_0 Free field green function
- h Radial distance between the trailing edge to the jet center line
- h_a Radial distance between the trailing edge opening to the jet center line
- k Wavenumber
- k_h Hydrodynamic wavenumber
- m Azimuthal mode
- M_a Acoustic Mach number
- r Distance between observer and source
- St Strouhal number
- T_{ii} Lighthill stress tensor
- U Flow velocity
- U_c Convective velocity
- w Opening width
- x Axial distance between the trailing edge to the nozzle exit
- x_c Position of maximum amplitude in the wavepacket

Julio A. Cordioli, Petrônio A. S. Nogueira, André V. G. Cavalieri, Maicon Secchi and William R. Wolf have contributed equally to this work.

Extended author information available on the last page of the article



- x_o Axial distance between the trailing edge opening to the nozzle exit
- α Fold angle
- θ Polar angle

1 Introduction

Installed jet noise is a practical problem with direct application in aircraft design, where in general both wing and engine are in close proximity. Modern aircraft have several highlift systems, and the configuration of these devices, such as flaps, slats and thrust gates (flaps openings in the region of the jet), can directly impact the safety, price and size of an aircraft (Van Dam 2002). The geometric configuration of an aircraft is also of great importance to the sound generation, especially for installed jet noise, since the distance between the jet and the wing can directly impact the radiated noise.

The noise generation phenomenon of a simple jet is well-founded in Lighthill's analogy (Lighthill 1952), which predicts the increase of sound power as a function of the eighth power of flow velocity. The Lighthill theory was applied to the turbofan engines in the 1960 s for estimating the reduction of Sound Power Level as a consequence of the reduced output mixing velocity (Smith 1989). Nevertheless, the problem of an installed jet is substantially more intricate due to the number of parameters playing a role in the phenomenon, such as the axial and radial distance between the trailing edge and the jet, as well as the geometry of the different surfaces involved. Furthermore, some surfaces change their position during different phases of the flight, such as the flaps, which have a low angle of deflection during cruise and a high angle during landing.

In general, installed jet noise can be divided in three categories: jet surface interaction (JSI), jet flap interaction (JFI) and jet surface reflection (JSR) (Lawrence 2014). The JFI case can be better described as a jet-trailing edge interaction (JTEI), as trailing edges of any aerodynamic surface can generate this phenomenon. This work will mainly study jet noise related to JSI, which means most of the energy involved in the process of sound generation is associated to the interaction between the acoustic near field and an aerodynamic surface.

Curle (1955) analyzed the problem of a solid body near a turbulent region and showed that the pressure fluctuations on the surface lead to a scattering effect when the acoustic field wavelength is greater than the surface dimensions. This effect can be described as a distribution of dipole-type sound sources that radiate noise more efficiently than the incident field quadrupole sources and, in this case, the sound power increases with the sixth power of flow velocity.

Ffowcs- Williams and Hall (1970) used Lighthill's analogy to analyze the acoustic scattering phenomenon for the case of an acoustic wavelength not necessarily greater than the surface dimensions. They analyzed the case of turbulent structures in the vicinity of a semi-infinite flat plate and showed that the sound power produced due to the scattering phenomenon in the trailing edge is proportional to the fifth power of the flow velocity. Indeed, JSI is mainly dominated by both phenomena described by Curle and Ffowcs-Williams and Hall and concentrates most of the acoustic energy in installed jets, especially for low Mach numbers. In the case when the wavelengths are much smaller than the surface dimensions, simple reflections will occur, and these reflection patterns can be predicted using ray tracing techniques, for instance.



In the case of scattering problems, it is convenient to simplify the geometries in order to better understand the fundamental phenomena being investigated. For example, a folded plate with an opening can be a simplification of a wing with a thrust gate. Several experimental studies have been carried out to understand and quantify the installed jet noise using flat plates (Brown 2013; Head and Fisher 1976; Lawrence et al. 2011). It is well documented that the proximity between the jet and the plate has a direct relation with the radiated noise to the far field. In the non-intrusive case, it is expected that the sound sources of the jet would not change, but the interaction of its acoustic near field with the surface will lead to the creation of "new sound sources", mainly as a result of scattering of the near-field energy to the far field, which otherwise would remain restricted to the near field. In the case of a flat plate, the relative position of the plate and the jet seems critical (Lawrence 2014; Podboy 2021). The further the plate is positioned downstream of the jet, the higher the contribution to low frequency part of the spectrum in the far field (Lawrence et al. 2011) due to the closer proximity to low frequency coherent turbulent structures. As expected, the radial distance between the jet and the plate controls the sound pressure increase in the far field due to the interaction in the near field (Cavalieri et al. 2013, 2014; Piantanida et al. 2016). Experiments have shown that the noise scattered in the trailing edge has phase opposition between the shielded and unshielded sides (Cavalieri et al. 2013), and the far-field noise has the shape of a dipole oriented perpendicular to the plate surface for the cases when the wavelength is greater than the geometry characteristic dimension (Head and Fisher 1976). In the cases with wavelength similar to the geometry dimensions different patterns can occur, like cardioid or patterns with several lobes (Cavalieri et al. 2014).

Based on these facts, it seems reasonable to expect a change in the directivity when the same geometry is positioned with other angles. For a large flat plate, this was confirmed experimentally, numerically and by using an analytical Green's function approximation for the case of a semi-infinite flat plate (Nogueira et al. 2019). In the case of folded plates, similar trends are expected, since the new noise sources are located at the nearest trailing edges. However, some questions may be raised related to the impact of the length of the folded parts (flap length) and the presence of openings (thrust gates), all of which are addressed in this work.

An initial study on the impact of flap trailing-edge on installed jet noise was presented by Mengle et al. (2007), which investigated experimentally the effect of serrated flaps and a mini vortex generator and observed reductions of the order of 1 dB. But even before that, different authors (Brown and Ahuja 1984; Way and Turner 1980; Sengupta 1983)have studied thrust gates, which are characterized by an opening on the flap used to minimise the interference between the engine flow and deployed flaps. These studies showed that openings equivalent to the nozzle exit diameter (DJ) provided noise reductions of around 5 dB (Brown and Ahuja 1984). More recently, Yupa-Villanueva et al. (2022) performed numerical analysis using a Lattice-Boltzmann commercial software, and two quantitative criteria were proposed for designing thrust gates in view of the reduction of jet-flap interaction noise. These findings highlight the importance of considering thrust gates as a significant factor in the study of installed jet noise and provide motivation for further research on their acoustic impact in aircraft design.

The main objective of this study is to evaluate the changes in the acoustic far field scattering by a folded plate when compared to a flat plate and how the radiated patterns can be modified when there is an opening in the folded part of the plate. Several openings are analyzed in order to clarify how the thrust gate width can be used to reduce the far field noise. These noise pattern variations are also investigated using a Boundary Element Method (BEM) with a wavepacket source which represents the incident sound generated by a jet.



The numerical methodology allows to further analyze the problem for angles not evaluated experimentally and is expected to have a reduced computational cost when compared to other approaches used in the literature (Yupa-Villanueva et al. 2022). Such reduced computational cost should allow the application of the numerical approach proposed as an effective design tool.

The work is organized as follows: Section 2 presents the basis of the wavepacket model adopted and the Boundary Element Method implementation used; in Sect. 3 the experimental setup is presented together with the cases that will be investigated through simulations and experiments; results and analyses are presented in Sect. 4. Finally, Sect. 5 summarizes the main conclusions of this work.

2 Mathematical Models

The main result of Lighthill acoustic analogy is the so-called Lighthill's stress tensor T_{ij} , which contains the information on the acoustic source based on the flow characteristics. The tensor can be written by a rearrangement of the Navier–Stokes equations (Lighthill 1952) and it reads as

$$T_{ii} = \rho u_i u_i + (p - \rho c^2) \delta_{ii} + \sigma_{ii}, \tag{1}$$

where ρ is the density, u_i is *i*th component of the velocity fluctuation, the term $(p - \rho c^2)$ is related to departures from isentropic behaviour, especially significant in heated jets, and σ_{ij} is related to the viscous effects.

For low Mach numbers and cold jets, the Lighthill stress tensor can be simplified, since the compressibility, viscous and entropic effects can be neglected in the sound generation process. As a result, the stress tensor becomes

$$T_{ij} \approx \rho_0 u_i u_j, \tag{2}$$

where one can note that its simplified version depends only of the velocity fluctuations. Here, the jet is treated as a distributed source and, in the present model, the low frequency contribution to the noise generation is predominant downstream the nozzle (Dougherty and Podboy 2009; Tam et al. 2008). On the other hand, near the jet exit, high-frequency content is more relevant and, in this context, the velocity fluctuations associated with the turbulent structures can be related to this spectral content. Crow and Champagne (Crow and Champagne 1971) visualized a series of hydrodynamic patterns in jets which grew, saturated and decayed in amplitude after some diameters axially, such as a hydrodynamic modulated wave. This mechanism can be modelled as a wavepacket that has the same pattern in its amplitude axially. For installed jet noise, such approach has had considerable success, predicting an exponential dependence of radiated sound with jet-edge distance (Cavalieri et al. 2014), and the reductions of JSI due to sweep (Piantanida et al. 2016) and angle of attack (Nogueira et al. 2019, 2017)E, as weel as the effect of an outer flight stream (Bychkov et al. 2022).

Therefore, instead of using the full Lighthill stress tensor as the source, which would have a high computational cost due to the use of detailed large-eddy simulations, an alternative is to model the acoustic source, or in this case the tensor, by a wavepacket (Crow 1972). Modal decomposition of the jet indicated that the axisymmetric mode (m = 0) is responsible for most of the acoustic energy measured at a low angles (Cavalieri et al. 2012). Using a wavepacket



model, a recent work showed that mode m = 0 represented most of the scattered sound by a plate (Nogueira et al. 2017), pointing out that the Lighthill tensor in the axial direction (T_{xx}) can also be considered to have a simple wavepacket shape in the form of

$$T_{xx} = Ar_c e^{-ik_h(x - x_c)} e^{-\left(\frac{x - x_c}{L}\right)^2},$$
(3)

where r_c is the cylinder radius, which is aligned with the jet nozzle lipline ($r_c = D/2$), k_h is the hydrodynamic wavenumber, x is the axial coordinate, x_c is the center of the wavepacket, L is the Gaussian envelope length and A is the amplitude that will be scaled with a measurement 30° downstream. The parameter k_h is calculated by $k_h = \omega/U_c$, where the convective velocity is $U_c = 0.9U$ and U is the jet exit velocity and $k_h L$ is chosen as 5 (Nogueira et al. 2019). The choice of convection velocity is representative of values for low Strouhal number St, as convection of large-scale axisymmetric structures occurs at values close to the jet velocity (Bechert and Pfizenmaier 1975; Jaunet et al. 2017) The value of wavepacket envelope length is consistent with observations from data from large-eddy simulations (Antonialli et al. 2023), which suggest values of the product $k_h L$ between 4.4 and 5.6 for subsonic jets. The wavepacket center is located around 6D, which was defined base on a calibration procedure with a baseline installed case. In order to calculate the acoustic pressure at a given position, a free-field Green's function can be used, which may be written as

$$G_0(\vec{x}, \vec{y}, k) = \frac{e^{-ik|\vec{x} - \vec{y}|}}{4\pi|\vec{x} - \vec{y}|},\tag{4}$$

where \mathbf{x} denotes an observer position, \mathbf{y} is a source position. The acoustic pressure for an individual acoustic wavenumber k can be computed by

$$p(k, \vec{x}) = \int_{V} G_0(\vec{x}, \vec{y}) \frac{\partial^2 \hat{T}_{ij}(k, \vec{y})}{\partial y_i \partial y_j} dV,$$
 (5)

where \hat{T}_{ij} represents the frequency domain Lighthill stress tensor.

Equation 5 can be used to calculate the incident pressure caused by the jet at any position, including over an aerodynamic surface, which in turn can be used as an input to a model based on the Boundary Element Method (BEM) (Wu 2002). The BEM allows the calculation of the scattered pressure by a surface of any geometry. The combination of the scattered sound pressure and the incident pressure at any observer gives the total pressure, which can be measured experimentally. The BEM equations can be obtained from the wave equation in the frequency domain using the Green's second identity, which leads to

$$C(\vec{x})p(\vec{x}) + \int_{S} \left[i\omega v_n G_0(\vec{x}, \vec{y}) + \frac{\partial G_0(\vec{x}, \vec{y})}{\partial n} \right] p(\vec{y}) dS = \int_{V} G_0(\vec{x}, \vec{y}) \frac{\partial^2 T_{ij}(\vec{y})}{\partial y_i \partial y_j} dV, \tag{6}$$

where $C(\vec{x})$ is equal to 0.5 if \vec{x} lies on a smooth boundary surface and equal to 1 outside of the surface, in the fluid where the acoustic propagation takes place. The term v_n refers to the particle velocity normal to the surface and $\frac{\partial G_0}{\partial n}$ can be expressed as $\vec{n} \cdot \nabla G_0$ which is the gradient of the Green's function in the normal direction of the surface element. In the case of a rigid surface, we can assume $v_n = 0$, so that the equation becomes



$$C(\vec{x})p(\vec{x}) + \int_{S} \frac{\partial G_0(\vec{x}, \vec{y})}{\partial n} p(\vec{y}) dS = \int_{V} G_0(\vec{x}, \vec{y}) \frac{\partial^2 \hat{T}_{ij}}{\partial_i \partial_i} dV.$$
 (7)

Initially, $p(\vec{y})$ is unknown on the surface and to find its value, which will be scattered to any observer, we can place the observer \vec{x} on the meshed surface using the collocational method (Wu 2002). There will be cases where the observer and the source lay on the same element, which will lead to the integral becoming singular; in these cases, a method to solve weak singularity is applied and the integral converges (Gaul et al. 2013; Wolf and Lele 2011). Repeating this process for every element, a system of equation is obtained and the surface pressure can be calculated by solving the linear system given by

$$[H]_{N \times N} \{ p_{surface} \}_{N \times 1} = \{ p_{incident} \}_{N \times 1}.$$
(8)

The matrix $H_{N\times N}$ is a fully populated matrix of complex valued terms where each component represents the impact of one element on another, which is evaluated by the surface integral. All the integrals are solved by Gaussian quadrature with three points in each direction of the surface element, totaling nine points in each element. Once $p(\vec{y})$ is found over the scattering surface, we can use Eq. 7 with $C(\vec{x}) = 1$ to calculate the pressure at any observer \vec{x} in the fluid domain.

As a consequence of the fully populated matrix in the BEM, the computational cost can become sometimes impractical, since the calculation time grows with $O(N^3)$, where N is the number of elements in the model. For the cases considered in this work, a mesh with 24 elements per wavelength was used, which resulted in almost 3000 elements to discretize the geometry, as can be seen in Fig. 1. For these cases, a simple desktop computer (i7 processor and 16 GB of RAM) was able to solve the problem in one hour. For larger cases with many more elements, the Fast Multipole Method can be used to reduce the computational cost (Wolf and Lele 2011).

The combination of BEM with the wavepacket model can be a powerful tool to analyze installed jet noise problems as shown by Cavalieri et al. (2014); Piantanida et al. (2016), and it provides some advantages to traditional CFD simulation, which leads to time consuming simulations and a large amount of data. On the other hand, the BEM/wavepacket model is not a high fidelity simulation and the users must be aware of its limitations. In general, this type of simulation can be done for the cases where the geometries are not intrusive, conserving the source model characteristics. Intrusion of an edge into the jet, with the trailing edge placed at a region with significant mean flow, may lead to slight departures from the model predictions (Piantanida et al. 2016), or to stronger effects such

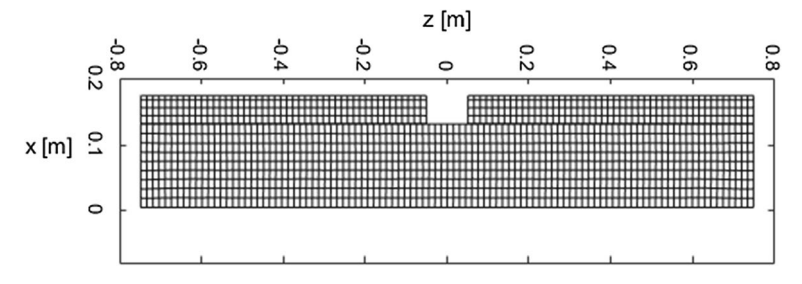


Fig. 1 A rectangular boundary element mesh on a folded plate with an opening used in one of the simulations



as resonance and the emission of tonal noise (Jordan et al. 2018), which are not predicted by the present method. With this in mind, the simulation can be used to evaluate several scattering problems involving jets and surfaces with complex geometries, such as flaps with thrust gates.

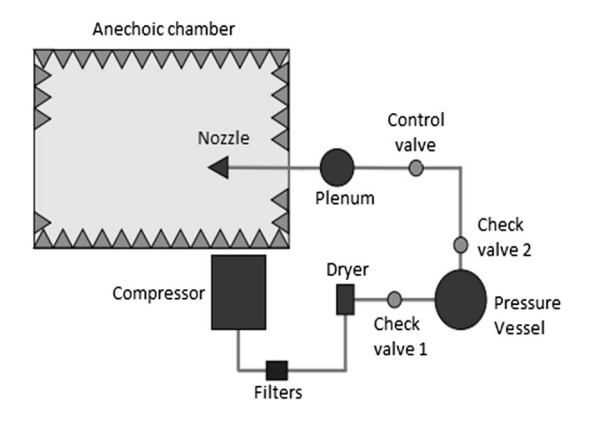
3 Experimental Setup and Simulation Cases

The experiment was performed at the Laboratory of Vibrations and Acoustics (LVA) of the Federal University of Santa Catarina, Brazil. The installation air line consists of a compressor, two filters, one dehumidifier, one pressure vessel for air supply, two locking valves, one control valve and a plenum for filtering the noise generated by the air line itself. The final pipeline is a duct of approximately 2 m length with a 2" diameter converging nozzle coupled. The nozzle used is a scaled nozzle based on the SMC 000. The rig has been verified and validated in previous studies Head and Fisher (1976), with results compared with other rig with the same nozzle design in cold subsonic conditions. The LVA/UFSC rig schematics is shown in Fig. 2.

The acoustic acquisition is done through 10 1/4" microphones located in the far field. The microphones are spaced equally on an arc that covers the polar angular positions from 30° downstream to 120° upstream. The arc has its center aligned with the center of the nozzle and it is at a radial distance of 41D, where D is the jet diameter. The airline system can reach Mach 0.9 for several seconds, but for the present investigations we chose to work at Mach 0.5, since the installation effect is more prominent at lower speeds. The acquisition is done using a sampling frequency of 120 kHz with a Hanning window and 75% of overlapping. The acoustic data is obtained for a frequency range of 10 Hz to 50 kHz in a narrow bandwidth of 10 Hz during 30 s. For small bandwidths, oscillations can appear in the spectrum and may lead to unclear patterns, when plotting the same frequency for several angles. To avoid this issue, the data is post processed to a bandwidth of 250 Hz.

For the installed jet tests, we used an aluminium plate of dimensions 1500 mm \times 170 mm \times 13 mm (width \times length \times thickness) with a mechanism that allows creating a fold at a specified angle. This foldable part has a length of 40.5 mm, and it is part of the total plate length. Another feature of the plate is an opening located at the center of this folding plate part. The opening can model the effect of a thrust gate in a wing and small pieces of the same material can be added for controlling the thrust gate width w, which has

Fig. 2 Schematics of the LVA's jet rig and its airline supply





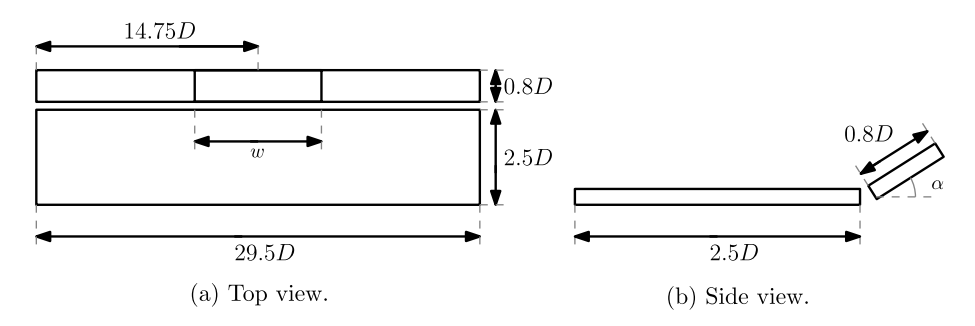


Fig. 3 Main dimensions of the folded flat plate used in the tests and details of the opening position and angle between the flat and folding parts

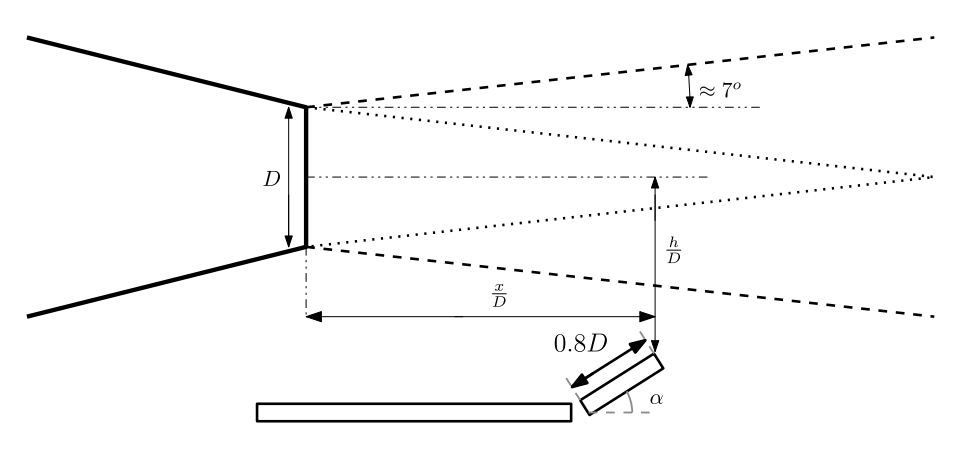


Fig. 4 Position scheme showing the dimensionless distances x/D and h/D

a maximum value of 3D. In the present study, we focus on the cases where w = 0.5D, 1D and 3D. For a better understanding, Fig. 3 shows the plate schematic and its features.

The experiments were performed at Mach number 0.5, for which the jet has an aperture of around 7°, such that at the axial distance of 3.3D, the jet plume has a radial support of 0.9D. Based on that, we decided to place the plate trailing edge at x/D = 3.3 and h/D = 1 avoiding significant intrusion that could trigger other mechanism not considered in the source model. The trailing-edge position was chosen carefully in order to have a relevant incident near field on the plate, avoiding the introduction of the geometry in the jet plume. This intend to avoid JTEI, which is not accounted in the simulation, while maximizing the effects of JSI, making this effect clear in the experiments. Figure 4 shows the position scheme. It is worth mentioning that in all experimental and simulation cases the trailing-edge position is the same, even when the fold angle (α) is modified.

In the cases with an opening in the center of the folded part, the distances h/D and x/D are not representative of the thrust gate trailing edge, which will be more distant than the trailing edge itself. For these cases we introduce the variables x_o and h_o which indicate the precise position of the thrust gate trailing edge. Two folding angles will be considered in the analysis, $\alpha = 0^\circ$ and 30° . These angles were chosen due to the different angles of attack of flaps during flight, for example in the takeoff the flaps assume a low deflection angle. On



the other hand, during the landing procedure, a high deflection angle is required. Besides that, we want to analyze how a 30° folding angle changes the directivity pattern of the scattered pressure to the far field, since it is already known that inclining the whole plate will change this pattern with a near rotation of the directivity in the same direction (Nogueira et al. 2019).

Table 1 summarizes the simulated and experimental cases with their position specifications and folding angles. The cases marked with the tag "*" represent the experimental cases. Not all the cases have associated measurements because the steps in the width opening are small, and it would be difficult to differentiate the experimental cases considering the measurement uncertainties.

Two baseline cases were chosen as references to allow the calculation of noise reduction from a full plate (no thrust gate) and the cases with an opening. The first baseline case is a simple flat plate and the second one is a folded plate with a folding angle of 30°. Cases 1 until 5 represent those setups with an opening, but no folding angle. Cases 6 until 11 are those with an opening and a folding angle of 30°. In these cases, the distance x_o differs from the previous cases. For $\alpha = 0$ ° the simulations were performed for the widths of 1D, 1.5D, 2D, 2.5D and 3D and only the cases of 1D and 3D have experimental data associated. On the other hand, for $\alpha = 30$ ° the simulations were performed for the widths of 0.5D, 1D, 1.5D, 2D, 2.5D and 3D, while comparison with experimental results are presented for the cases of 0.5D, 1D and 3D.

As in previous works (Cavalieri et al. 2014; Antonialli et al. 2023), it was necessary to perform a calibration of the kinematic wavepacket model with experimental data. The calibration of the source was made in two steps: first we used the experimental data of an isolated jet to calibrate the free amplitude A of the wavepacket source for Strouhal number 0.22, such that its sound radiation for the free jet matches experimental results for the microphone at angular position of 30°.. The center of the wavepacket (x_c) was adjusted using the "Baseline 1" case at the same Strouhal number. After this calibration no change in the model parameters were made. The wavepacket model used in this work only considers mode 0 and neglects the effect of jitter/coherence decay (Sirotto et al. 2018), which has a consequence in the phase at the far field. Since we wanted to use this simplified model

Table 1 Parameters of simulated and experimental cases (experimental cases marked with *)

Setup	x/D	h/D	x_0/D	h_0/D	α	w
Baseline 1*	3.3	1.0	_	_	0°	_
Case 1*	3.3	1.0	2.5	1.0	0°	1
Case 2	3.3	1.0	2.5	1.0	0°	1.5
Case 3	3.3	1.0	2.5	1.0	0°	2
Case 4	3.3	1.0	2.5	1.0	0°	2.5
Case 5*	3.3	1.0	2.5	1.0	0°	3
Baseline 2*	3.3	1.0	_	-	30°	_
Case 6*	3.3	1.0	2.6	1.4	30°	0.5
Case 7*	3.3	1.0	2.6	1.4	30°	1
Case 8	3.3	1.0	2.6	1.4	30°	1.5
Case 9	3.3	1.0	2.6	1.4	30°	2
Case 10	3.3	1.0	2.6	1.4	30°	2.5
Case 11*	3.3	1.0	2.6	1.4	30°	3
Case 12	2.6	1.4	_	-	0	_



and we were not able to calibrate the phase, the scattered pressure and the source pressure will be treated as uncorrelated fields.

4 Results and Discussion

We start the analysis by comparing the power spectral densities (PSDs) for an isolated jet and an installed jet for the Baseline 1 setup (see Table 1). The main objective of this comparison is to confirm that the position x/D=3.33 and h/D=1 allows the observation of the installation effects for the present case. If the installation effects are not substantial for the baseline case, it will be difficult to evaluate some patterns, like directivity rotation and noise reduction, since all the phenomena we are looking for are related to installation effects. Figure 5 shows the results for this test at two polar angles. The comparison shows that the installed jet displays higher sound levels for upstream angles when compared to the isolated jet, resulting in a gain of over 10 dB/St around a Strouhal number of 0.3. This validates the position as a good choice to study changes in the spectra of the installed jet when the geometry is modified. The trends observed follow previous results discussed in the literature (Lawrence et al. 2011; Lawrence 2014), with installation effects being more relevant at upstream angles, especially for low Strouhal numbers, and downstream positions being dominated by pure jet noise. For higher frequencies, the installation effects tend to decay to a simple reflection effect.

Based on Fig. 5, the simulations will be carried on at St = 0.22 where the installation effect is close to its maximum. For this Strouhal number, the wavepacket model was calibrated to match the PSD evaluated at angular position of 30° , allowing the identification of the radiation patterns generated by the source and the scattered acoustic field by the plate due to the incident pressure. Figure 6 shows the directivity patterns for both the source alone and the scattered acoustic field in polar coordinates.

The wavepacket source with only azimuthal mode 0 is a super directive source as can be seen in the pattern shown in Fig. 6. The incident pressure of this distributed source is scattered by the plate to other angles and, as can be seen, the acoustic scattered pattern for this low Strouhal number is similar to a dipole as predicted by Curle (1955). The summation of

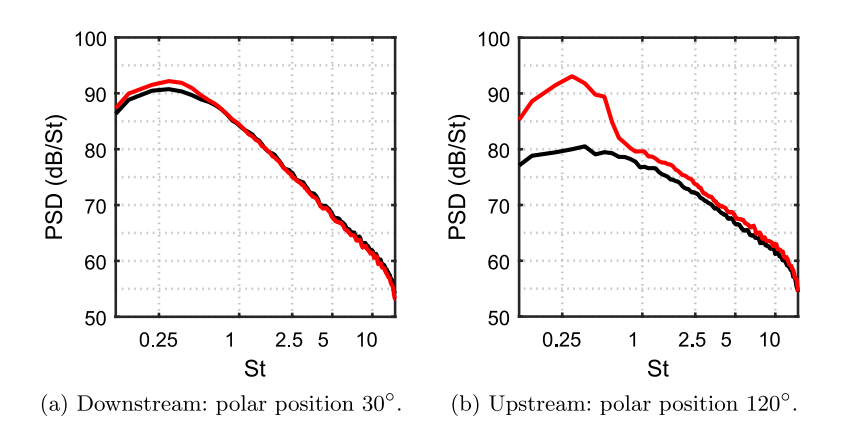


Fig. 5 Measured acoustic far-field for an isolated (black) and an installed jet (red) for the baseline position x/D = 3.33 and h/D = 1



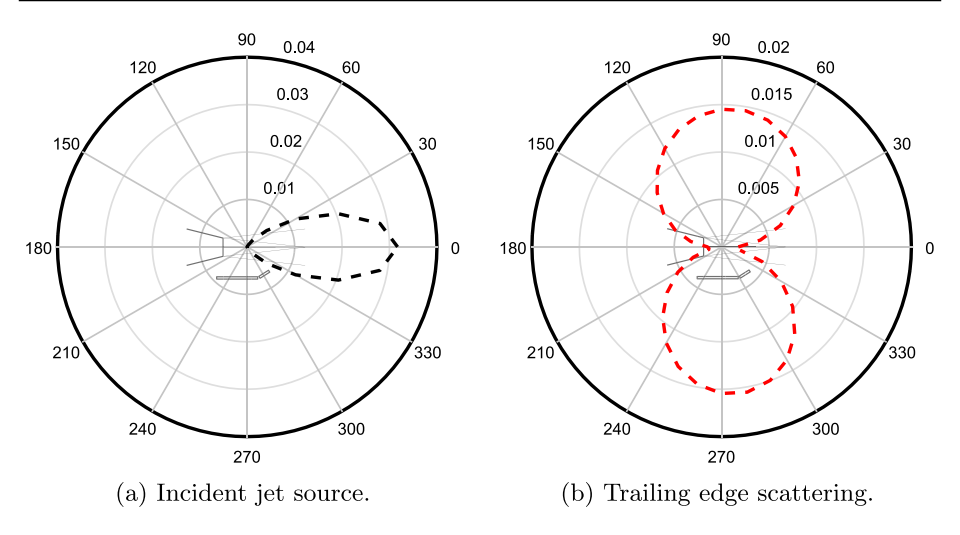


Fig. 6 Far-field acoustic pressure directivities of incident source (jet) and scattered source (trailing edge)

direct acoustic field (incident source) and the scattered acoustic field can be then compared to the acoustic pressure captured by a microphone in the far field. Figure 7a shows the total acoustic pressure for several angles together with the experimental data, while Fig. 7b provides a zoom for the angles evaluated at the experiments. Overall, a very good agreement between the simulation and the measured values can be observed. In terms of absolute values, the discrepancy between the simulation and the experimental data is always less than 1 dB/St.

The scattered acoustic field is directly related to the incident pressure at the plate surface, which is shown in Fig. 8 for BEM results. It can be noted that the highest pressure levels, almost 25 dB/St above other levels, are located at the central part of the plate unshielded side and close to the trailing edge of the plate. This information explains part of

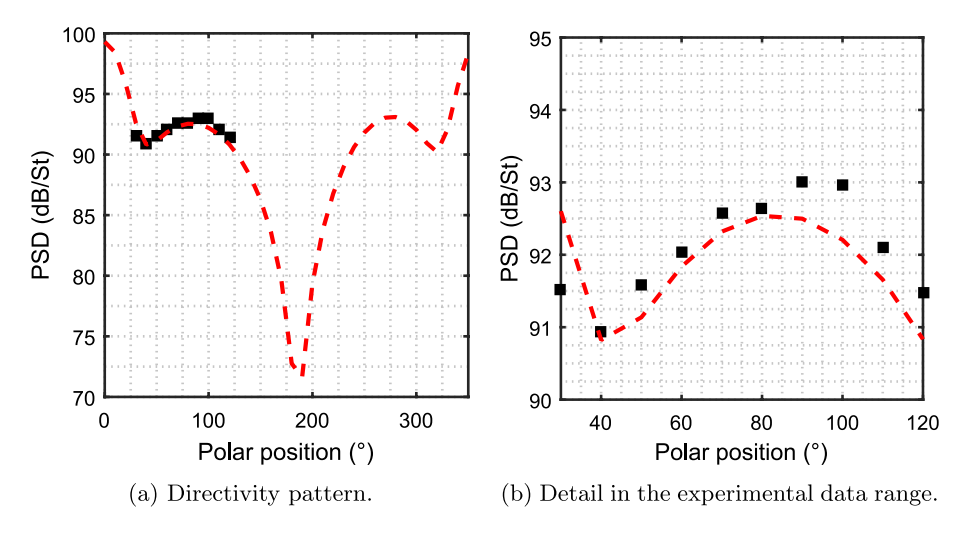


Fig. 7 Comparison between experimental data (black) and simulations (red) for the case Baseline 1

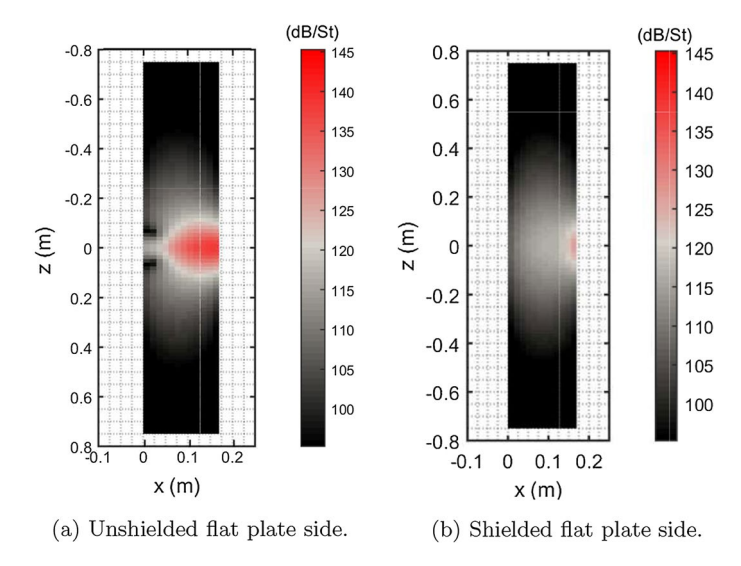


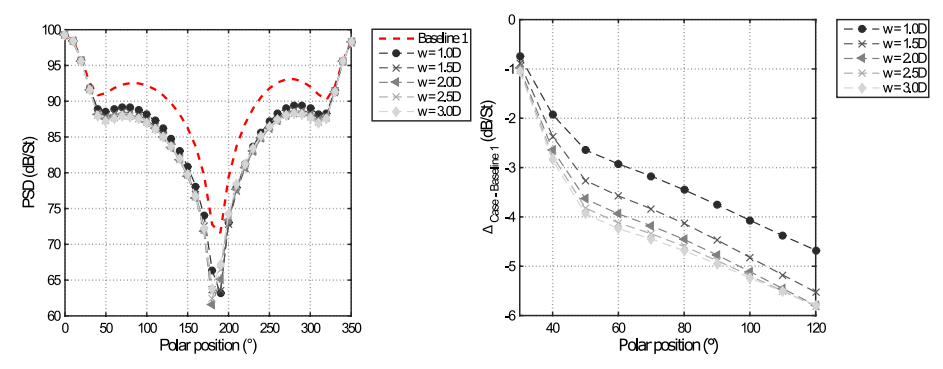
Fig. 8 Pressure levels on both sides of the plate that were calculated using the BEM

the phenomena associated to the rotation of the directivity pattern of the scattered sound, since most of the acoustic energy is concentrated in this region. The distance between the wavepacket peak and the surface plays an important role in how the pressure is distributed over the surface, showing once again the importance of a careful study of the placement of surfaces, such as wings, close to turbulent jets. As shown in Fig. 8, the region of high amplitudes extends about $0.20 \, \mathrm{m}$ (or 4D) in the z direction, totaling only 13% of the plate total width. Therefore, a significant noise reduction may be obtained by modifying only a small part of the plate, with a reduced aerodynamic penalty. In our simplified model, this is equivalent to modifying a portion of the foldable part of the plate. A simple modification can be done by just opening a space in this region, which will increase the distance between the trailing edge of this central part and the source, while reducing the pressure levels in the region.

Several openings were simulated, as described in Table 1. Cases 1 to 5 were simulated and compared with the case Baseline 1, and results are shown in Fig. 9. To better evaluate the reduction due the openings, the differences between these cases and that of the baseline one are also calculated and presented for analysis. The results show a very similar pattern and similar PSD reductions for any aperture simulated. This indicates that even small openings in the central part of the plate can have a significant contribution to the reduction of the scattered noise to the far field for a 0° folding angle, and there is no relevant benefit that compensates larger openings above a width of 2D.

The results in Fig. 9 indicate a reduction in the order of 1 dB/St for downstream angles, which is expected since these angles are dominated by the jet incident field. More substantial reductions are reached for upstream angles, reaching up to 5 dB/St. The results between different openings do not differ on more than 1.5 dB/St. To verify this trend, simulation and the experimental results are compared in Fig. 10. Overall, the reductions found in the simulations are in very good agreement with the experiments for most angles. At upstream angles the simulations seem to slightly overestimate the reduction. The only exception are the results for w = 3D, with simulation over predicting the reductions. A possible





(a) Total pressure for setups baseline 1 (b) Delta between baseline 1 setup and and cases 1 to 5.

Fig. 9 Simulation results for cases with 0° of folding angle

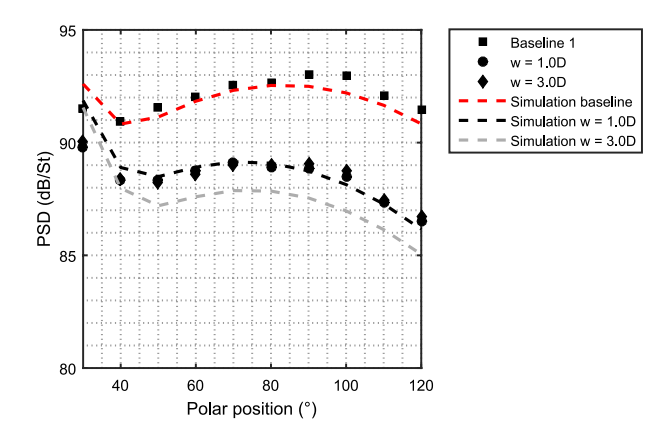


Fig. 10 Simulation and experimental data for the Baseline 1 setup and cases 1 and 5

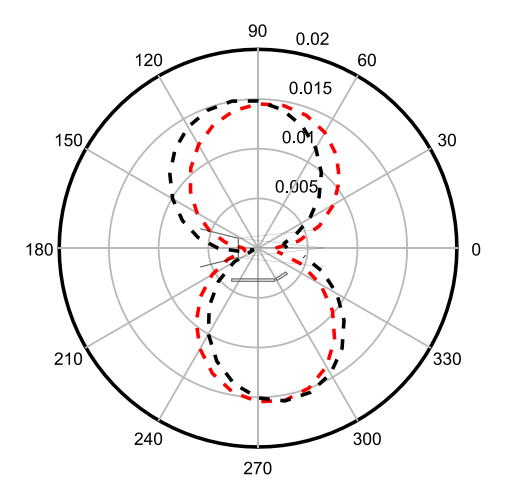
explanation for this behavior is that the experimental incident pressure field at the plate may be more concentrated within 1D of the span, leading to negligible reductions as w is increased.

The next step is to analyze the case of a flat plate with a nonzero folding angle at the trailing edge. We expect to observe a phenomenon similar to the one described in previous works (Nogueira et al. 2019), where an approximate rotation of the scattered directivity pattern was seen. Since the plate scattering has a dipolar shape for low frequencies, with silence zones aligned with the leading and trailing edge directions, we expect a rotation of the scattered directivity in an angle between 0° (angle of the leading edge) and the folding angle (for this case, 30°). Figure 11 shows the simulated directivity pattern of the baseline cases 1 ($\alpha = 0^{\circ}$) and 2 ($\alpha = 30^{\circ}$).

The simulations indicate a rotation of the dipole directivity, confirming the predominance in the far-field patterns related to the trailing-edge angle. The rotation angle was about 20° for the peak. With the folding part (flap) redirecting the noise, the central region of the flap has a fundamental role in the far-field sound pressure levels. In the case of an



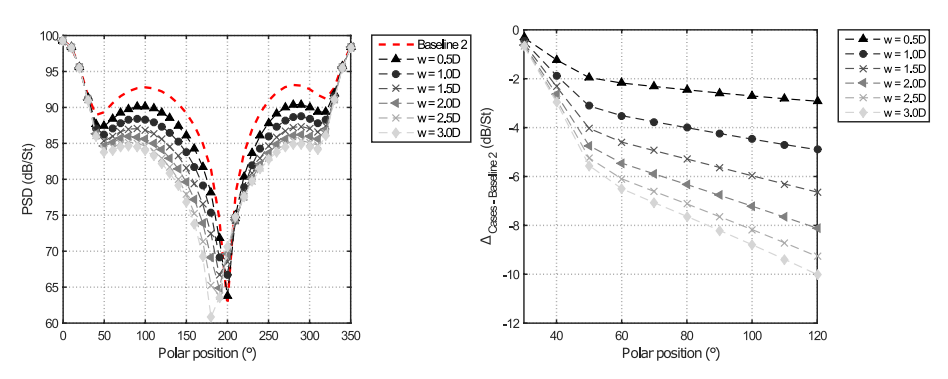
Fig. 11 Scattered directivity pattern for cases Baseline 1 (red) and Baseline 2 (black)



opening (thrust gate), the trailing edge of the flap in the central region is further away from the jet than the trailing edge of the rest of the flap structure, as indicated in Table 1 by the parameters x_o/D and h_o/D . Since the interaction has an exponential dependence (Cavalieri et al. 2014), we expect more attenuation for the cases with openings.

Figure 12 displays the scattered pressure field for cases 6 to 11. The differences between these cases and the Baseline 2 setup are also shown in the same figure. As expected, the results for $\alpha=30^\circ$ are different when compared to the flat plate cases, since the vertical distance between jet and trailing edge for these cases are not the same. For the cases with $\alpha=30^\circ$, we can note a more significant noise reduction in the far field. At low angles the reductions are negligible, but in the region dominated by the scattered sound field, the reduction generated by the inclusion of a thrust gate ranges from 2 dB/St, for the case of an opening of 0.5D, to almost 10 dB/St, for the larger opening at $\theta=120^\circ$. In order to confirm these patterns, Fig. 13 shows the comparison with the experimental data.

Once again, experimental data and the simulation results display a very good agreement both in magnitude and curve shape. For the Baseline 2 setup and cases 6 and 7, the errors between experiments and model are within 1 dB/St for most angles. For the case with an



(a) Total pressure for the Baseline 2 and (b) Delta between the Baseline 2 and cases 6 until 11. other cases.

Fig. 12 Simulation results for cases with 30° of folding angle



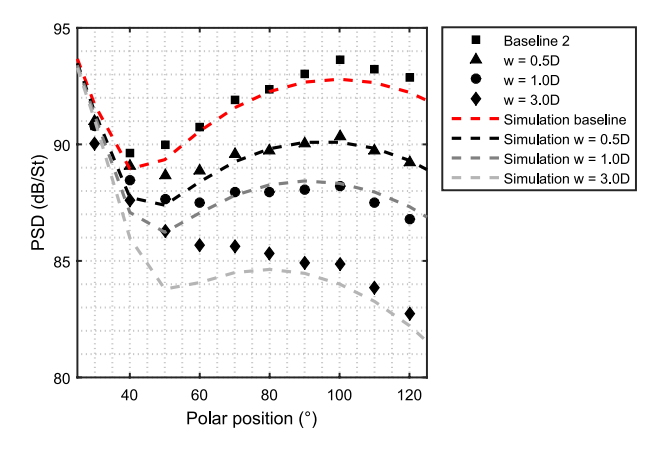


Fig. 13 Simulation and experimental data for the case Baseline 2 and cases 6, 7 and 11

opening of w = 3D, especially in the region of angular position from 50° until 70°, the discrepancies between experimental and simulation data are slightly higher. This may be due to the random nature of the source, which does not create a perfect dipole pattern (the minimum at around 50° is associated with the dipole), or due to the intrinsic limitations of simplifying the turbulent source term to a simple analytical wavepacket with a single azimuthal wavenumber. It is interesting to note that the 10 dB/St reduction at 120° is confirmed by the experimental data.

In order to evaluate the total noise reduction resulting from the flap openings, the Overall Sound Pressure Level (OASPL) is calculated based on the simulation and experimental data. Only angles from 30° to 120° from the simulation data are considered in this calculation, since those are the angles evaluated experimentally. The OASPL was computed for each opening width. Figure 14 illustrates the trend for both numerical and experimental data for the cases considered in this work ($\alpha = 0^{\circ}$ and $\alpha = 30^{\circ}$). Overall, numerical and

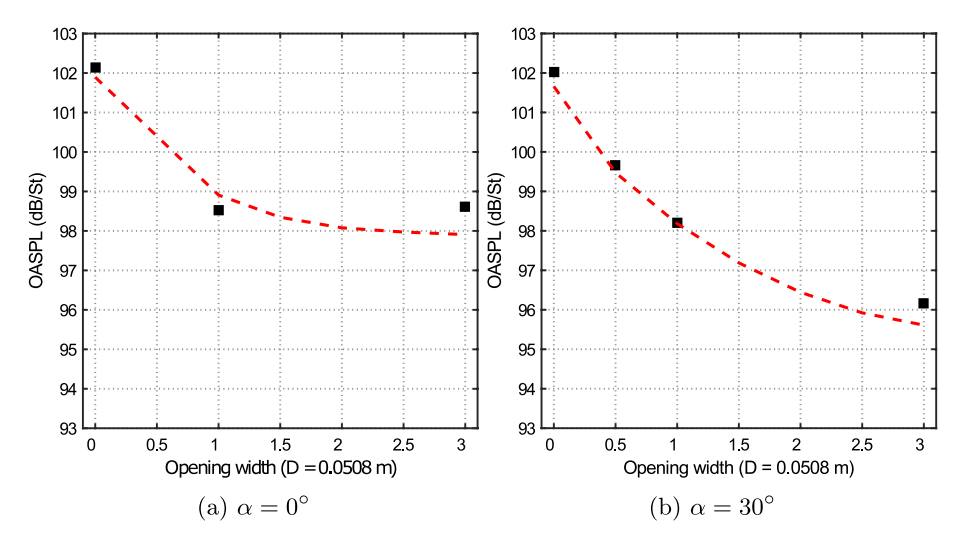


Fig. 14 OASPL trends for several openings shown for experimental data (black) and simulation results (red)

experimental results agree very well for both cases. It can be seen that for the case of $\alpha=0^{\circ}$ openings greater than 1D do not have a global reduction impact. This trend is similar to the one shown in Fig. 9. On the other hand, for $\alpha=30^{\circ}$ the openings have a increasing impact on noise reduction up to 3D. However, extrapolating the curve, it seems that larger openings will not result in a relevant impact, with the levels reaching an asymptotic behavior. Indeed, an opening of 1D width reduced the OASPL around 4 dB/St, while an opening width three times greater only provides an additional 2 dB/St of noise reduction.

In order to analyze the directivity patterns formed by the scattered and the total sound pressure, the levels are calculated at the surface of a sphere around the center of the exhaust nozzle. For this, a new BEM simulation is carried on, and the observation points are defined every 5 degrees. The radius of the sphere is defined as equal to the radius of the arc of microphones used in the previous simulations and experiments. Figures 15 and 17 show the result obtained in a lateral view (xy plane) with the middle point of the plate leading edge at the position (x = 0, y = 0).

The results displayed in Fig. 15 suggests that the trailing edge delimits the silence region (shown in blue in the figures).. It can be observed that the silence region is inclined in the case of no thrust gate and as openings are made, the composition between the plate trailing edge and the bottom of the thrust gate dictates a new silence region. In the cases where the trailing edge of the central region of the plate displays higher pressure levels than the trailing edge of the flap, the silent region is aligned with the plate.

It can also be noted from the sound pressure captured over the sphere, as larger thrust gates openings were used, the levels tend to decrease. The existing directive pattern, assigned to the flap, is also modified with larger opening thrust gates. For a large thrust gate opening (Case 11, w = 3D), a dipole pattern is again aligned with the surface. This is an indication that the behavior for large openings tends towards a simple flat plate in a new position. This case was also simulated and the result is displayed in Fig. 16, which compares case 11 (original plate with thrust gate with w = 3D and $\alpha = 30^{\circ}$) and case 12 (reduced flat plate).

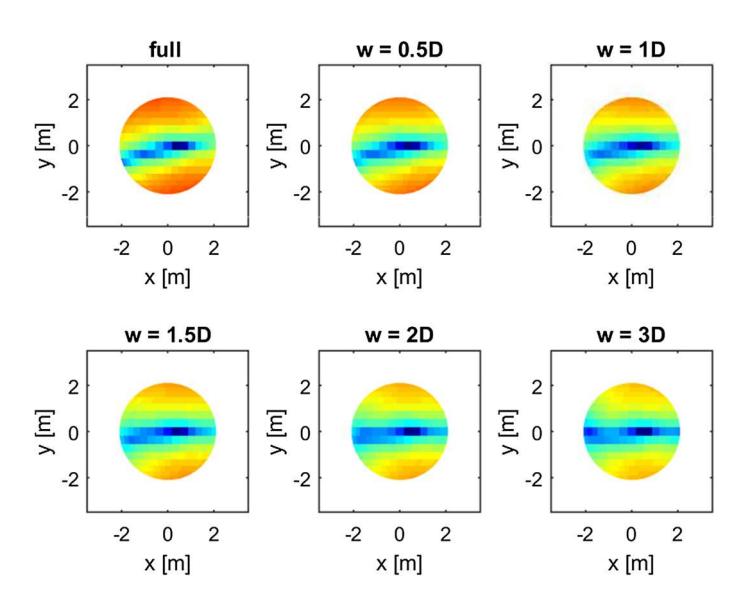


Fig. 15 Scattered sound levels for the case Baseline 2 and cases 6, 7, 8, 9 and 11



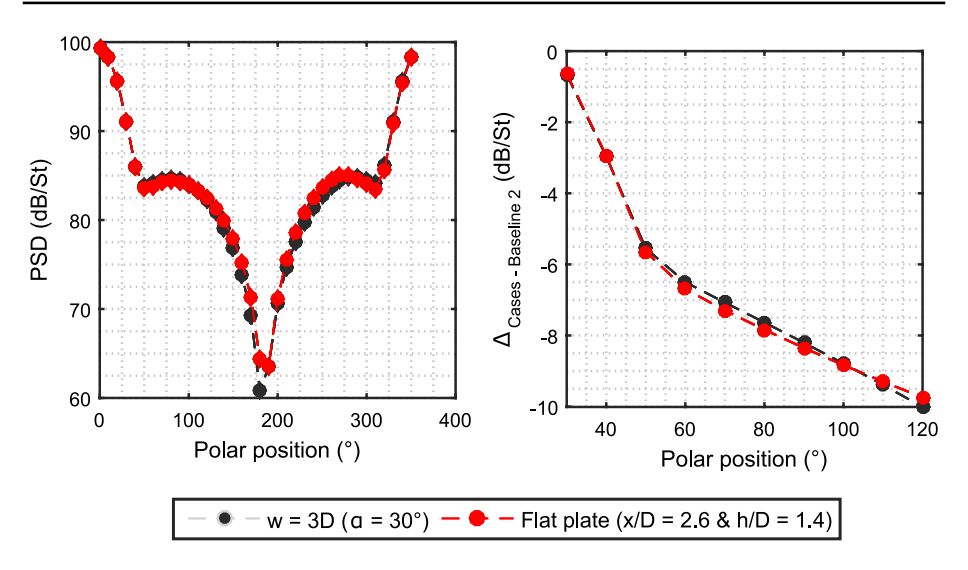


Fig. 16 Sound pressure level for cases 11 (black) and 12 (red), and noise reduction when compared to case Baseline 2

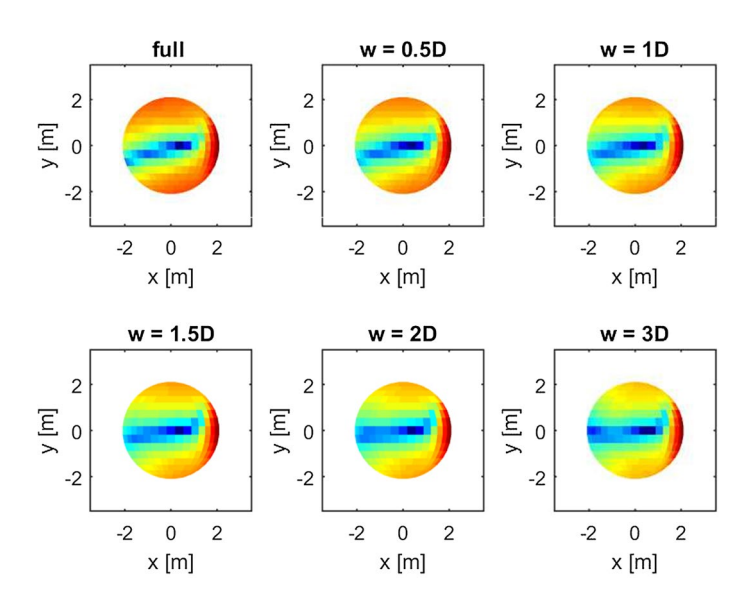


Fig. 17 Pressure sound level for the case Baseline 2 and cases 6, 7, 8, 9 and 11

The simulation result shows a high agreement between both cases, confirming that the main scattered pressure is related to the flat plate trailing edge, which means the flap does not have a important role when a 3D thrust gate is inserted. The distance between the source and the trailing edge, in that region, is smaller than the distance between the source and the flap. Since the source intensity has an exponential decay in the radial direction, it leads to a significant decrease in the scattered pressure at the far-field.



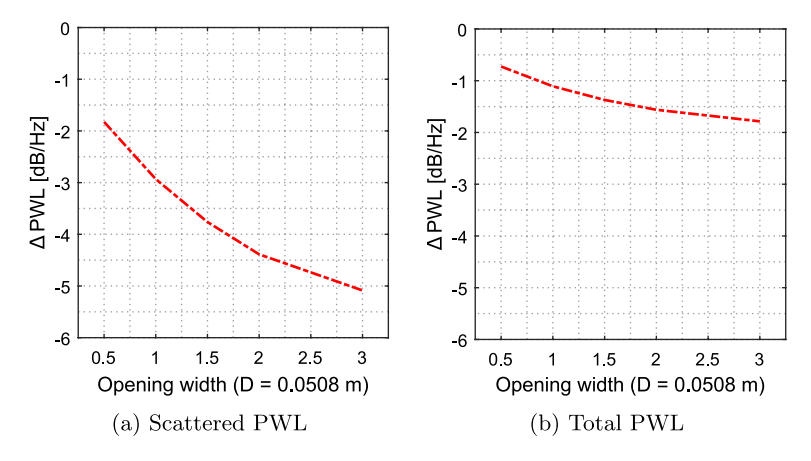


Fig. 18 Calculation of $\triangle PWL$ trends for several openings (w/D)

Figure 17 shows the composition between the sound source and the noise scattered at the sphere surface. The upstream noise is little altered by the downstream sound source, which is superdirective, and the conclusions previously stated for the installation noise are not altered. For the case of no thrust gate, the installation noise and the source noise are similar, however, for thrust gates of relevant apertures the dominant noise becomes the isolated jet noise.

As a next step, the sound power was calculated using the pressure scattered over the sphere position. Figure 18 shows the behavior for the sound power reduction for an installed jet without a thrust gate in comparison with the use of thrust gates, for (a) scattered PWL and (b) total PWL.

The results are very similar to those observed for the sound pressure levels, but emphasizes that the decay of the scattered sound power and the total sound power is also present when other azimuthal angles are considered. Again, the scattered sound power changes significantly with apertures, even though increasingly larger apertures are needed to produce the same power decay. The total sound power, in turn, has a different decay, since the sound source is not altered by the openings, in this way the first openings are effective in the reduction and the subsequent ones have little impact. The simulation indicates a 5 dB/St reduction for the scattered pressure, and a reduction of 2 dB/St for the total pressure using a 3D span thrust gate. These results show that geometric modifications made to the wing flap assembly can have relevant effects in reducing installation noise.

5 Conclusions

The jet-installation noise studies performed in this work intended to mimic, in a simplified way, the installation noise from a jet in the proximity of a wing-flap system with a thrust gate. Several simulations and experiments were performed to evaluate the impact of the thrust gate in the acoustic far field. The simulations were performed using the BEM with a simplified wavepacket model for the source. Two baseline cases were considered: the case of a flat plate and a folded plate, in order to evaluate the differences in the directivity patterns at the far field. By means of the numerical results, it was possible to observe a



dipole rotation related to the folding angle. Cases with different thrust gate widths were then simulated, and some of these cases had their results compared with experimental data. In general, a very good agreement between numerical and experimental data was observed. Substantial noise reductions were found for the cases of openings in the folded plate at the far field for St=0.22, for which installation noise is more significant. It is believed that these reductions are due to a combination of effects; besides the opening itself, the distance between the trailing edge of the thrust gate and the source seems to play an important role. A trend close to an exponential decay of global noise reduction related to the opening width was also found through simulation and experimental data.

The present results show how simplified wavepacket models coupled with BEM, by capturing the dominant sound-generation mechanism, may be a viable approach for the design of quieter jet-wing geometries. Our choice of rectangular openings representing thrust gates was motivated by its simplicity, but could nonetheless lead to significant reductions of radiated sound in the experiments, which were correctly predicted by BEM. It is likely that other thrust gate geometries may be beneficial to mitigate installation effects, and further explorations using the wavepacket-BEM approach may suggest novel geometries to reduce sound radiation. This may be coupled with further aerodynamic analysis, aiming at finding geometries that reduce sound radiation without compromising aerodynamic efficiency of high-lift devices.

Acknowledgements The authors thank the support provided by EMBRAER S.A. and Finep by means of the project SILENCE. J.R.L.N.S. and P.A.S.N. were funded by scholarships from the National Council for Scientific and Technological Development—CNPq. J.R.L.N.S thanks Dynamox S.A. for the time provided during the production of this article. J.A.C. acknowledges support from CNPq under Grant 315000/2021-0. W. R. W. acknowledges support from FAPESP under Grant 21/06448-0. The authors thank the support from Lucas A. Bonomo on the production of some figures.

Author Contributions JRLNS was responsible for the work conceptualization, definition of the methodology, software implementation and validation, experimental tests, formal analysis and investigation of the results and writing the original draft. JAC was responsible for the work conceptualization, definition of the methodology, funding, formal analysis and investigation of the results, writing the original draft, review and editing. PASN was responsible for the work conceptualization, definition of the methodology, formal analysis and investigation of the results, original draft, review and editing of the manuscript. AVGC was responsible for the work conceptualization, definition of the methodology, formal analysis and investigation of the results, original draft, review and editing of the manuscript. MS was responsible for the work conceptualization, definition of the methodology, formal analysis and investigation of the results, original draft, review and editing of the manuscript. WRW was responsible for the work conceptualization, definition of the methodology, formal analysis and investigation of the results, original draft, review and editing of the manuscript. WRW was responsible for the work conceptualization, definition of the methodology, formal analysis and investigation of the results, original draft, review and editing of the manuscript.

Funding The present work was funded by EMBRAER S.A. and Finep by means of the project SILENCE. J.R.L.N.S. and P.A.S.N. were funded by a CNPq scholarship. J.R.L.N.S thanks Dynamox S.A. for the time provided during the production of this article. J.A.C. acknowledges support from CNPq under Grant 315000/2021-0. W. R. W. acknowledges support from FAPESP under Grant 21/06448-0. No further funding is associated with this work.

Declarations

Conflict of interest The authors have no competing interests to declare that are relevant to the content of this article.

Ethical Approval The authors have no relevant financial or non-financial interests to disclose.

Informed Consent All of the material, including data and figures, is owned by the authors and no permissions are required.



References

- Van Dam, C.: The aerodynamic design of multi-element high-lift systems for transport airplanes. Progr. Aerosp. Sci. 38(2), 101–144 (2002)
- Lighthill, M.J.: On sound generated aerodynamically i general theory. Proc. R. Soc. London Ser. A Math. Phys. Sci. 211, 564–587 (1952)
- Smith, M.J.: Aircraft Noise. Cambridge University Press, UK (1989)
- Lawrence, J.: Aeroacoustic interactions of installed subsonic round jets. PhD thesis, University of Southampton (2014)
- Curle, N.: The influence of solid boundaries upon aerodynamic sound. Proc. R. Soc. London Ser. A Math. Phys. Sci. 231(1187), 505–514 (1955)
- Williams, J.F., Hall, L.: Aerodynamic sound generation by turbulent flow in the vicinity of a scattering half plane. J. Fluid Mech. **40**(4), 657–670 (1970)
- Brown, C.A.: Jet-surface interaction test: far-field noise results. J. Eng. Gas Turb. Power **135**(7), 071201 (2013)
- Head, R., Fisher, M.: Jet/surface interaction noise-analysis of farfield low frequency augmentations of jet noise due to the presence of a solid shield. In: 3rd AIAA Aeroacoustics Conference, p. 502 (1976)
- Lawrence, J., Azarpeyvand, M., Self, R.: Interaction between a flat plate and a circular subsonic jet. In: 17th AIAA/CEAS Aeroacoustics Conference (32nd AIAA Aeroacoustics Conference), p. 2745 (2011)
- Podboy, G.G.: Jet-Surface Interaction Test: Phased Array Noise Source Localization Results vol. 44670. NASA/TM-2013-218085, USA (2012)
- Cavalieri, A.V., Wolf, W.R., Jordan, P., Gervais, Y.: Diffraction effects of finite and semi-infinite flat plates in the vicinity of a turbulent subsonic jet. In: 22nd International Congress of Mechanical Engineering (COBEM 2013) (2013)
- Cavalieri, A.V., Jordan, P., Wolf, W.R., Gervais, Y.: Scattering of wavepackets by a flat plate in the vicinity of a turbulent jet. J. Sound Vibr. 333(24), 6516–6531 (2014)
- Piantanida, S., Jaunet, V., Huber, J., Wolf, W.R., Jordan, P., Cavalieri, A.V.: Scattering of turbulent-jet wavepackets by a swept trailing edge. J. Acoust. Soc. Am. 140(6), 4350–4359 (2016)
- Nogueira, P.A., Sirotto, J.R., Miotto, R.F., Cavalieri, A.V., Cordioli, J.A., Wolf, W.R.: Acoustic radiation of subsonic jets in the vicinity of an inclined flat plate. J. Acoust. Soc. Am. **146**(1), 50–59 (2019)
- Mengle, V., Stoker, R., Brusniak, L., Elkoby, R., Thomas, R.: Flaperon modification effect on jet-flap interaction noise reduction for chevron nozzles. In: 13th AIAA/CEAS Aeroacoustics Conference (28th AIAA Aeroacoustics Conference), p. 3666 (2007)
- Brown, W., Ahuja, K.: Jet and wing/flap interaction noise. In: 9th Aeroacoustics Conference, p. 2362 (1984) Way, D., Turner, B.: Model tests demonstrating under-wing installation effects on engine exhaust noise. In: 6th Aeroacoustics Conference, p. 1048 (1980)
- Sengupta, G.: Analysis of jet-airframe interaction noise. In: 8th Aeroacoustics Conference, p. 783 (1983)
- Yupa-Villanueva, R.M., da Silva, F.D., Deschamps, C.J.: Quantitative criteria for designing thrust gates to mitigate jet-flap interaction noise. Applied Acoustics **200**, 109076 (2022)
- Dougherty, R., Podboy, G.: Improved phased array imaging of a model jet. In: 15th AIAA/CEAS Aeroacoustics Conference (30th AIAA Aeroacoustics Conference), p. 3186 (2009)
- Tam, C.K., Viswanathan, K., Ahuja, K., Panda, J.: The sources of jet noise: experimental evidence. J. Fluid Mech. 615, 253–292 (2008)
- Crow, S.C., Champagne, F.: Orderly structure in jet turbulence. J. Fluid Mech. 48(3), 547–591 (1971)
- Nogueira, P.A., Cavalieri, A.V., Jordan, P.: A model problem for sound radiation by an installed jet. J. Sound Vibr. **391**, 95–115 (2017)
- Bychkov, O., Faranosov, G., Kopiev, V., Soares, L.F., Cavalieri, A.V.: Jet installation noise modeling in static and flight conditions using centerline fluctuations. AIAA J. 60(6), 3620–3634 (2022)
- Crow, S.: Acoustic gain of a turbulent jet. Springer, New York (1972)
- Cavalieri, A.V., Jordan, P., Colonius, T., Gervais, Y.: Axisymmetric superdirectivity in subsonic jets. J. Fluid Mech. 704, 388–420 (2012)
- Bechert, D., Pfizenmaier, E.: On wavelike perturbations in a free jet travelling faster than the mean flow in the jet. J. Fluid Mech. **72**(2), 341–352 (1975)
- Jaunet, V., Jordan, P., Cavalieri, A.: Two-point coherence of wave packets in turbulent jets. Phys. Rev. Fluids 2(2), 024604 (2017)
- Antonialli, L.A., Cavalieri, A.V., Nogueira, P.A., Sirotto, J.R., Cordioli, J.A.: Prediction of installed jet noise from wave-packet models tuned with freejet data. AIAA J. 61(4), 1749–1758 (2023)
- Wu, T.: Boundary Element Acoustics Fundamentals and Computer Codes. Acoustical Society of America, USA (2002)



- Gaul, L., Kögl, M., Wagner, M.: Boundary Element Methods for Engineers and Scientists: an Introductory Course with Advanced Topics. Springer, Germany (2013)
- Wolf, W., Lele, S.: Wideband fast multipole boundary element method: application to acoustic scattering from aerodynamic bodies. Int. J. Numer. Methods Fluids 67(12), 2108–2129 (2011)
- Jordan, P., Jaunet, V., Towne, A., Cavalieri, A.V., Colonius, T., Schmidt, O., Agarwal, A.: Jet-flap interaction tones. J. Fluid Mech. 853, 333–358 (2018)
- Sirotto, J.R., Cordioli, J.A., Cavalieri, A.V.: Analysis of far-field coherence of subsonic jet noise. In: 2018 AIAA/CEAS Aeroacoustics Conference, p. 2977 (2018)

Springer Nature or its licensor (e.g. a society or other partner) holds exclusive rights to this article under a publishing agreement with the author(s) or other rightsholder(s); author self-archiving of the accepted manuscript version of this article is solely governed by the terms of such publishing agreement and applicable law

Authors and Affiliations

José R. L. N. Sirotto¹ · Julio A. Cordioli² · Petrônio A. S. Nogueira³ · André V. G. Cavalieri⁴ · Maicon Secchi⁵ · William R. Wolf⁶

☐ Julio A. Cordioli julio.cordioli@ufsc.br

José R. L. N. Sirotto jose.neto@dynamox.net

Petrônio A. S. Nogueira petronio.nogueira@monash.edu

André V. G. Cavalieri andre@ita.br

Maicon Secchi maicon.secchi@gmail.com

William R. Wolf wolf@fem.unicamp.br

- Business Intelligence Coordinator, Dynamox S.A., R. Parque Tecnológico Alfa, Módulo 05, Florianópolis, SC 88030-909, Brazil
- Mechanical Engineering Department, Federal University of Santa Catarina, Campus Universitário, Florianópolis, SC 88040-900, Brazil
- Department of Mechanical and Aerospace Engineering, Monash University, Clayton, VIC 3800, Australia
- Divisão de Engenharia Aeronáutica, Instituto Tecnológico de Aeronáutica, São José dos Campos, SP 12228-900, Brazil
- Aeroacoustics Engineer, Archer, 190 W Tasman Dr, San Jose, CA 95134, USA
- School of Mechanical Engineering, University of Campinas, Campinas, SP 13083-860, Brazil

